Sediment yield error correction by dynamic system response curve method in real-time flood forecasting

Lu Hou, Weimin Bao, Wei Si, Peng Jiang, Peng Shi, Simin Qu and Fanghong Ye

ABSTRACT

Real-time flood forecasting requires accurate and reliable estimates of the uncertainty to make efficient flood event management strategies. However, the accuracy of flood forecasts can be severely affected by errors in the estimates of sediment yield in the loess region. To improve the accuracy of sediment-laden flood forecasts generated using streamflow-sediment coupled (SSC) model, an error feedback correction method based on the dynamic system response curve (DSRC) is proposed. The physical basis of the system response curve is the sediment concentration of the hydrological model. The theoretical basis of the method is the differential of the system response function of the sediment yield time series. The effectiveness of DSRC method is evaluated via an ideal case and three real-data cases with different basin scales of the Yellow River. Results suggest that the DSRC method can effectively improve the accuracy and stability of sediment transport forecasts by providing accurate estimates of the sediment yield errors. The degree of forecast improvement is scale dependent and is more significant for larger basins with lower rain gauge densities. Besides, the DSRC method is relatively simple to apply without the need to modify either the model structure or parameters in real-time flood forecasting.

Key words | dynamic system response curve, error correction, real-time flood forecasting, streamflow-sediment coupled model, Yellow River basin

Lu Hou
Weimin Bao
Wei Si (corresponding author)
Peng Jiang
Peng Shi
Simin Qu
Department of Hydrology and Water Resources,
Hohai University,
Nanjing,
China
E-mail: *siwei@hhu.edu.cn*

Wei Si
Yellow River Institute of Hydraulic Research,
Zhengzhou 450003,
China

Fanghong Ye
Hydrology Station,
Lishui of Zhejiang Province,
Lishui,
China

HIGHLIGHTS

- Slope sediment yield error has been corrected through the DSRC method coupled with the SSC model. The DSRC method is relatively simple to apply and can improve the accuracy and stability of real-time model predictions without increasing either model complexity and/or the number of model parameters. The SSC model is simple, the model parameters are easily calibrated, and the model structure is physics-based.

INTRODUCTION

The loess region of the Yellow River is famous for its characteristics of high sediment loads and transport. Before-storm and raindrop splash soil erosions are the original sources for suspended sediment yield. These two processes usually provide enough loose soil at most locations due to the distinctive soil properties (Xian *et al.* 1983; Fang *et al.* 2008). Runoff, which is in response to rainfall events, acts directly on the sediment transportation (Hairsine *et al.* 1999; Jiao *et al.* 2002; Nearing *et al.* 2005; Rouhipour *et al.* 2006; Wu *et al.* 2018). To give better understanding of the physical law of flow and sediment transport in the loess region, a streamflow-sediment coupled (SSC) model with

doi: 10.2166/hydro.2020.203

clear physical meaning, simple structure and parameters was established by Bao (1995). Numerous attempts have been made to illustrate the proposed SSC model is rational and applicable in forecasting streamflow-sediment processes within the loess region (Bao *et al.* 2019; Si *et al.* 2017). However, flow simulation always shows relatively higher accuracy than the simulation of sediment transport processes at both event and annual temporal scales.

Sediment generation is a complex function of climate, hydrology, basin topography and land cover (Bingner *et al.* 1997; Merritt *et al.* 2003; De Vente & Poesen 2005; De Vente *et al.* 2010; Rompaey *et al.* 2010; Si *et al.* 2016). In-channel proximal deposits of sediment make significant contributions to the total sediment load. Sediment distal supply and proximal sediment availability are strongly related with the time-varying streamflow and erosion/deposition processes (Si *et al.* 2017; Juez *et al.* 2018a, 2018b). Many factors influence the forecasting result, among which the sediment yield error dominates the volume error which directly affects the accuracy of sediment transport estimates. A widely used approach to reduce the size of forecast errors is real-time error correction (Babovic *et al.* 2001; De Chant & Moradkhani 2012; Bao *et al.* 2014; Chen *et al.* 2015; Si *et al.* 2019). According to different corrected variables, error correction is classified into four categories (WMO 1992): input, state, parameters, and output correction. Different methods have been proposed for the correction of different variables. For example, the AR model (Pegram & James 1972; Babovic *et al.* 2001; Komma *et al.* 2008; Ju *et al.* 2009) is commonly used for output correction. However, mutation occurs around the flood peak and the errors there are not correlated, which leads to unreasonable results when using the AR model (Bao 2006). Besides, either an Ensemble Kalman Filter (EnKF) or Particle Filter (PF) can be used to recursively update the model states and parameters via data assimilation (Vrugt *et al.* 2006; Weerts *et al.* 2006; Neal *et al.* 2009; De Chant & Moradkhani 2012; Moradkhani *et al.* 2012). The results show that the EnKF is consistently overconfident in predicting streamflow.

In view of this, a dynamic system response curve (DSRC) method is proposed to update estimates of the inputs, state variables and outputs. Much subsequent experience supports its validity for updating flow at the outlet in hydrological models. For instance, the DSRC method is compared with the AR model in correcting both input and state errors, including free-water storage (Bao *et al.* 2015), soil water content, rainfall (Si *et al.* 2013a, 2015, 2016, 2019; Yang *et al.* 2015) and runoff (Si *et al.* 2013b; Bao *et al.* 2014; Zhang *et al.* 2014; Liu *et al.* 2015). The DSRC method always presents better performance without requiring modifications to model structure (Gupta *et al.* 2012) or parameters calibration (Gupta *et al.* 2008). Thus, updating real-time flood forecasts based on system differential response theory is of increasingly high value for real-time error correction studies. The DSRC method has the dominant features of clear physical concept (Bao *et al.* 2014), simple structure and stable performance (Si *et al.* 2015, 2019). It can provide an effective and stable correction for the outputs without losing the lead time. Existing studies have paid more attention to updating the real-time flood forecasting by correcting streamflow phase errors, while little attention has been given to the sediment transport phase, of which the accurate predictions are critically informative for efficient reservoir operation, river management, flood control, and warning in the Yellow River basin (Zhang *et al.* 2007; Tamene *et al.* 2010; Palazon *et al.* 2014). Therefore, investigation of those errors resulting from uncertainties in the sediment transport simulation is needed.

The objective of this paper is to employ the DSRC method coupled with the SSC model for improving the accuracy of sediment prediction results through correcting the sediment yield time series in the loess region. The physical basis of the system response curve is the sediment concentration of the SSC model. The theoretical basis for using DSRC – to correct the error of slope sediment yield – is the differential of the system response function of the slope sediment yield time series (Si *et al.* 2015, 2019). This proposed method is tested in three steps: (1) an ideal case is selected to demonstrate the applicability of the DSRC method using the SSC model; (2) three real basins with different scales in the Yellow River are used to further test the method performance and provide insights into correction effectiveness; (3) the initial calculated and the corrected forecasts are compared by further contrastive analyses using certain performance indices. Results show that the new correction approach is reasonable and effective

for forecast-updating, and can result in improved prediction accuracy.

STUDY AREA

Sediment in the Yellow River mainly comes from the midstreams which are rich in sediment. Therefore, three different scale basins in the middle reach of the Yellow River basin with 101 historical floods are selected to further test the proposed error feedback correction method based on the DSRC. Jiuyuangou basin (the area is 70.7 km^2), which is a tributary in the middle reaches of Wuding River with 11 rainfall stations, is located between latitudes 37°33N and 37°38N, longtitudes 110°16E and 110°26E. The annual mean precipitation is about 500 mm, of which 70% is concentrated in the flooding season (from June to September). The mean modulus of soil erosion varied from 18,000 to 19,900 $t/km^2 \cdot a$ during the natural period (Wang *et al.* 2016a). Since the year 1953, considerable soil and water conservation management has been carried out across the basin, and more strikingly, the dam system emerged (Wang *et al.* 2016b). It is recorded that during the period of the 1970 and 1980s, check-dams rapidly developed up to over 250, whose total storage capacity reached 0.43 million m^3.

Chabagou basin is a larger tributary of the Dali River, which belongs to the first sub-area of hilly and gully in loess plateau, with a drainage area of 187 km^2 and 46 rainfall stations. Caoping hydrological station is an important controller at the basin outlet. The average annual precipitation in the basin is about 447 mm, 80% of the total precipitation, which is more concentrative spatially and temporally from June to September with high intensity. High sediment loads of flood are linked to obvious changes to the annual runoff and sediment transport (Qi *et al.* 2011), with an erosion modulus of almost 222,000 $t/km^2 \cdot a$. Check-dams have been constructed in the Chabagou watershed and boomed in the 1970s before stagnating after the 1980s (Zhang *et al.* 2010), which depressed the sediment yield by reducing the frequency and intensity of hyper-concentration streamflow and soil erosion in gullies.

Dali River basin is the largest tributary of the Wuding River, with a drainage area of 3,906 km^2 and 67 rainfall stations. Sparse vegetation coverage, fragmented terrain and the dry climate cause serious water and soil loss in the loess plateau and further contribute to the majority of sediment in the Yellow River in the form of suspended sediment. In the late 1980s, more than 3,100 dams were built for water and soil conservation within the basin. The annual mean precipitation in this basin is 439.5 mm in the form of torrential rain. Because of the weak erosion resistance resulting from the low-level management before the 1970s, the average sediment transport modulus was 16,000 $t/km^2 \cdot a$ (Qi *et al.* 2011). Suide hydrological station is the major control station at the outlet of Dali River basin.

Precipitation across all study basins is characterized by small scope, short duration and high intensity. Severe soil erosion, therefore, is a result of rainstorm in the loess region. Moreover, the annual distribution of precipitation is extremely uneven, accompanied by significant interannual variation. Precipitation in the flooding season (from May to September) accounts for more than 80% of the total annual precipitation. Sediment loads caused by rainstorms are much higher than those caused by common rainfall and are more concentrated in the flooding season than the dry season. The locations of rainfall and hydrological stations in these study basins are shown in Figure 1(a)–1(c).

METHOD AND MATERIALS

Streamflow-sediment coupled model

The proposed sediment yield model is coupled with a conceptual hydrologic model. It has a simple structure and specific physical meaning. The model has been successfully applied in the watersheds with similar soil texture to that of the loess plateau region (Bao *et al.* 2019). Therefore, the SSC model is chosen to study the streamflow-sediment simulation and forecasting in the loess region in the middle reach of the Yellow River.

The characteristic feature of the SSC model is the concept of hydraulic erosion capacity and soil erosion resistance capacity, and the distribution curve of soil erosion resistance capacity. Detachment and deposition along the flow path are integrated results determined by time-varying

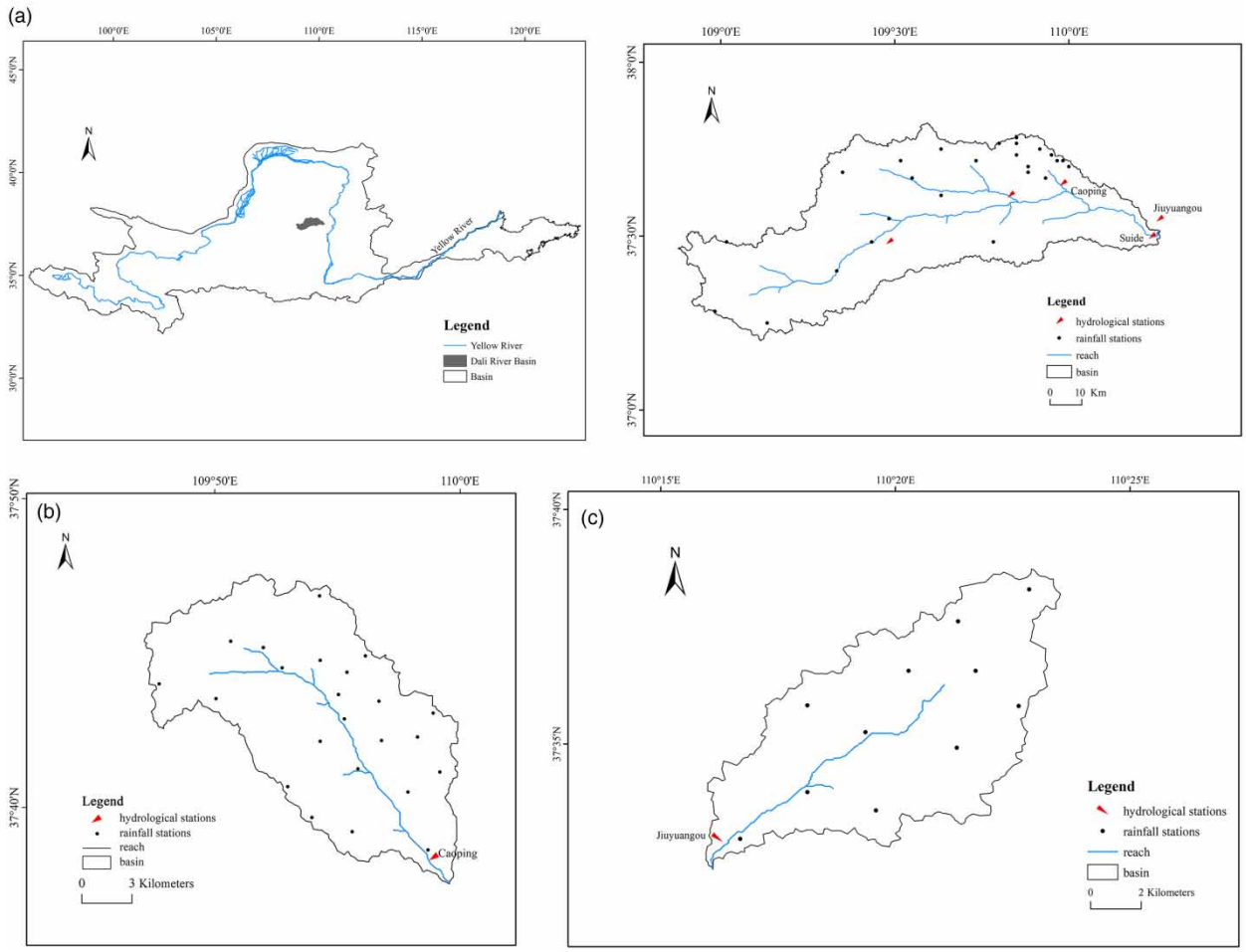

Figure 1 | Site distribution map of the study basins. (a) Dali River basin, (b) Chabagou basin, (c) Jiuyuangou basin.

hydraulic factors, as well as sediment distal supply and proximal sediment availability (Si *et al.* 2017; Juez *et al.* 2018a, 2018b). Thus, an event responsive watershed sediment generation structure and conceptual structure of sediment movement in gully and stream are established. The SSC model is divided into the following five parts:

(1) Runoff generation: The vertically-mixed runoff generation method combines the spatial distribution curve of infiltration capacity with the water storage capacity curve (Bao & Wang 1997). Runoff (R) is generated when rainfall (P) hits the ground, and in general is initially separated into surface runoff and infiltration streamflow through the spatial distribution curve of infiltration capacity. The infiltration streamflow (RR), including subsurface and groundwater runoff, replenishes soil moisture deficiency generated by the evapotranspiration. Underground runoff is generated where the soil moisture content of the aeration zone reaches field capacity. Surface runoff formation in the excess of infiltration is determined by rainfall intensity and infiltration; and, on the other hand, subsurface and groundwater runoff generation upon repletion of storage are dependent on early soil water shortage and the volume of infiltration.

(2) Separation of runoff components: The free water reservoir division method (Bao *et al.* 2019) is applied to divide the previously determined total runoff into three components: surface runoff (RS), subsurface runoff (RI), and groundwater runoff (RG).

(3) Streamflow concentration: The three runoff components are further transferred into QS, QI, and QG, and

together form the total inflow to the channel network of the sub-basin. The outflow of the sub-basin is Q. By applying the Muskingum method to successive sub-reaches (Zhao 1993), flood routing from sub-basin outlets to total basin outlets is achieved. Eventually, the discharge (TQ) is obtained.

(4) Sediment generation: According to the proposed spatial distribution curve of soil erosion resistance capacity (Si *et al.* 2017; Bao *et al.* 2019), slope sediment yield (SS) could be acquired by the integral of the difference between sediment carrying capacity and soil erosion resistance capacity. Gully sediment generation (SG), which varies with the hydraulic condition of the channel, is calculated by the suspended sediment formula of Bagnold's River channel (Bagnold 1960). Due to the parameter CGM (channel sediment concentration on average) based on the physical meaning, the relationship between hydraulic factors and the sediment yield rate of gully erosion is well explained (Bao *et al.* 2019). Slope and gully sediment generation together form the total suspended sediment load within the stream section.

(5) Sediment transport: The transport capacity is the threshold for erosion and deposition (Si *et al.* 2017). If the actual sediment concentration is less than its capacity, erosion occurs; otherwise, deposition occurs. The corresponding coefficient ξ is introduced to reflect the erosion and deposition relationship. By referring to the similarity of streamflow concentration, sediment transportation in the stream section is calculated by sediment continuity and motion equation. The slope and gully sediment yield are further collected into TSS and TSG. Finally, the sediment process at the total basin outlet (TS) is obtained by continuous routing.

The structural diagram of the SSC model is shown in Figure 2. The symbols inside the blocks are variables including inputs, outputs, state variables, and internal variables while those outside are parameters. The inputs of the model are rainfall (P) and measured pan evaporation (EM). The outputs are the discharge (TQ), the sediment transport rate (TS) from the whole basin and the actual evapotranspiration (E), which includes three components, EU, EL, and ED. The state variables are the area mean tension water storage (W) and the area mean free water storage

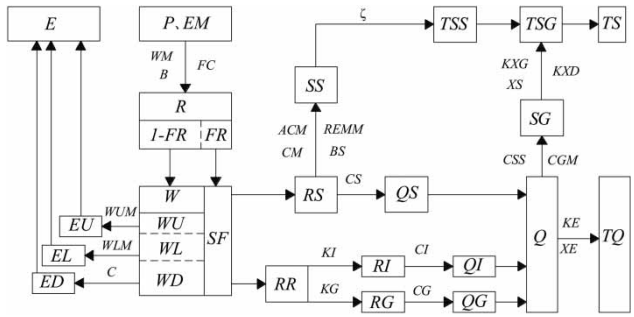

Figure 2 | Flowchart for the streamflow-sediment coupled model.

(SF). The area mean tension water (W) had three components (WU, WL, and WD) in the upper, lower, and deep layer. FR is the runoff contributing area factor that is related to W. The rest of the symbols inside the blocks are all internal variables. The functions, methods, parameters meaning and corresponding value ranges of streamflow and sediment part are shown in Tables 1 and 2 respectively. More detailed calculation formula and the physical explanation of each parameter are illustrated in Bao *et al.* (2019).

Dynamic system response curve

To apply the DSRC method, the SSC model is systematically generalized into a nonlinear response system except for the parts before sediment generation (Figure 3). The dashed box is the system used for slope sediment yield correction in this study. Because this correction is affected by the values of sediment yield at other times, it is time-varying, and the system response curve is dynamic.

The generalized system in Figure 3 can be conceptualized as

$$\boldsymbol{S}(t) = \boldsymbol{S}[\boldsymbol{X}(t), \theta, t] \tag{1}$$

where $\boldsymbol{S}(t) = [S_1, S_2, \cdots, S_L]^T$ is a time-ordered vector of sediment transport rate at the outlet; $\boldsymbol{X}(t)$ is the corresponding vector of various variables in the model (input variables, intermediate state variables); θ is the vector of model parameters; and t is time.

Any slight changes in each parameter and variables in Equation (1) will affect the sediment transport processes at the outlet of the basin. The model parameters θ are calibrated and determined by the observed data of various

Table 1 | Parameters in streamflow calculation

Streamflow calculation

Function	Evapotranspiration	Runoff generation	Runoff separation	Streamflow concentration	
Method	Three-layer evaporation pattern	Vertical mixed runoff method	Free water storage reservoir	Linear reservoir	Muskingum method
Meaning of parameter and its value range	*K*: ratio of potential evapotranspiration to pan evaporation (0.2–1.0) *WUM*: tension water capacity of upper layer (10–20) *WLM*: tension water capacity of lower layer (60–80) *C*: coefficient of deep evapotranspiration (0.1–0.2)	*WM*: areal mean tension water capacity (180–350) *FC*: average steady infiltration rate of watershed (0.1–10) B: exponent of the tension water capacity distribution curve (0.1–1.0)	*KI*: outflow coefficients of interflow (0.3–0.4) *KG*: outflow coefficients of groundwater (0.1–1.0)	*CS*: recession constant in the "lag and route" method (0.10–0.65) *CI*: recession constant of interflow storage (0.65–0.95) *CG*: recession constant of groundwater storage (0.1–1.0)	*KE* and *XE* are parameters of the Muskingum method, which can be initially determined by hydraulic formulas (0.05–0.55)

Table 2 | Parameters in sediment calculation

Sediment calculation

Function	Slope sediment generation	Slope sediment transportation	Gully sediment generation	Stream sediment erosion	Stream sediment transportation
Meaning of parameter and its value range	*ACM*: coefficient of hydraulic erosion capacity on slopes (0.001–1) *CM*: maximum sediment concentration of slope streamflow in the whole basin (5–2000) *REMM*: maximum erosion resistance of watershed (>0) *BS*: distribution curve index of erosion resistance (0.1–5)	ξ: scour and deposition coefficient (0.01–1)	*CGM*: average sediment yield concentration in gully (>0) *CSS*: rill erosion coefficient (0.1–250)	*KXD*: dynamic nonlinear coefficient of scouring and deposition (0.1–0.999)	*KXG*: average propagation time of sediment particles in river reach (0.2–3) *XS*: proportion coefficient (0.1–0.55)

basins with different characteristics by an optimum algorithm (Bao *et al.* 2013), and are considered to be time-invariant (Si *et al.* 2015). Accordingly, changes to the processes of surface erosion and sediment yield are dependent primarily on inputs (areal mean rainfall and potential evapotranspiration) and streamflow conditions, which are critical factors in the simulation of the sediment transport process. In this study, we consider that changes in outflow are caused primarily by changes in the slope sediment yield time series. So Equation (1) can be simply expressed as:

$$\boldsymbol{S}(t) = \boldsymbol{S}[\boldsymbol{SS}, \theta, t] \tag{2}$$

where $\boldsymbol{SS} = [ss_1, ss_2, \cdots, ss_n]^T$ is the vector of time-ordered series of slope sediment yield. Differentiation by slope

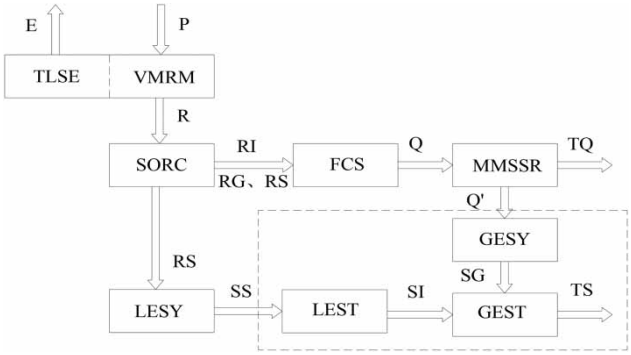

Figure 3 | Generalized system diagram of streamflow-sediment coupled model (*TLSE*, three-layer evapotranspiration; *VMRM*, vertically-mixed runoff generation; *SORC*, separation of runoff components; *FCS*, different components flow concentration in the slope; *MMSSR*, Muskingum method to successive sub-reaches; *LESY*, slope erosion and sediment yield; *LEST*, slope sediment concentration; *GESY*, gully erosion and sediment yield; *GEST*, represents channel sediment concentration).

sediment yield as an independent variable expression of the equation is:

$$d\boldsymbol{S}(\boldsymbol{SS}, \theta, t) = \frac{\partial \boldsymbol{S}}{\partial \boldsymbol{SS}}|_{\boldsymbol{SS}=\boldsymbol{SS}_C} d\boldsymbol{S} \tag{3}$$

where $\boldsymbol{SS}_C = [ss_{C1}, ss_{C2}, \cdots, ss_{Cn}]^T$ is the time-ordered vector of the primary value of calculated slope sediment yield. $\frac{\partial \boldsymbol{S}}{\partial \boldsymbol{SS}}$ is a sensitivity coefficient of the system response when the slope sediment yield series is $\boldsymbol{SS}_C$.

$$d\boldsymbol{S} = \frac{\partial \boldsymbol{S}(\boldsymbol{SS}, \theta, t)}{\partial ss_1}|_{\boldsymbol{SS}=\boldsymbol{SS}_C}\Delta ss_1 + \frac{\partial \boldsymbol{S}(\boldsymbol{SS}, \theta, t)}{\partial ss_2}|_{\boldsymbol{SS}=\boldsymbol{SS}_C}\Delta ss_2 + \cdots + \frac{\partial \boldsymbol{S}(\boldsymbol{SS}, \theta, t)}{\partial ss_n}|_{\boldsymbol{SS}=\boldsymbol{SS}_C}\Delta ss_n \tag{4}$$

If the sample length of observed sediment transport rate is L, $\boldsymbol{S}(t) = [S_1, S_2, \cdots, S_L]^T$ is substituted into Equation (4) and expressed as:

The matrix form of Equation (5) can be expressed as:

$$\boldsymbol{S}(\boldsymbol{SS}, \theta, t) = \boldsymbol{S}(\boldsymbol{SS}_C, \theta, t) + \boldsymbol{U}\Delta\boldsymbol{SS} + \boldsymbol{E} \tag{6}$$

where $\boldsymbol{SS}_C = [ss_{C1}, ss_{C2}, \cdots, ss_{Cn}]^T$ is the vector of time-ordered series of slope sediment yield primarily calculated by the model; $\boldsymbol{S}(\boldsymbol{SS}_C, \theta, t)$ is the initial series of calculated sediment transport rate; $\Delta\boldsymbol{SS} = [\Delta ss_1, \Delta ss_2, \Delta ss_3, \cdots]^T$ is the vector of time-ordered series of slope sediment yield error estimated by the least squares required solution; $\boldsymbol{E} = [e_1, e_2, \cdots, e_L]^T$ is the stochastic residuals of observed sediment transport rate, which is the white noise vector subject to a zero-mean Gaussian distribution; $\boldsymbol{U}$ is the matrix of dynamic system response, which can be expressed as:

$$\boldsymbol{U} = \begin{bmatrix} \frac{\partial \boldsymbol{S}(\boldsymbol{SS}, \theta, 1)}{\partial ss_1} & \cdots & \frac{\partial \boldsymbol{S}(\boldsymbol{SS}, \theta, 1)}{\partial ss_n} \\ \vdots & \vdots & \vdots \\ \frac{\partial \boldsymbol{S}(\boldsymbol{SS}, \theta, L)}{\partial ss_1} & \cdots & \frac{\partial \boldsymbol{S}(\boldsymbol{SS}, \theta, L)}{\partial ss_n} \end{bmatrix} \tag{7}$$

Each item in the matrix $\boldsymbol{U}$ can be solved by the differential approximation of Equation (8):

$$\frac{\partial \boldsymbol{S}(\boldsymbol{SS}, \theta, t)}{\partial ss_i} = \frac{\boldsymbol{S}((ss_1, \cdots, ss_i + \Delta ss_i, \cdots), \theta, t) - \boldsymbol{S}((ss_1, \cdots, ss_i, \cdots), \theta, t)}{\Delta ss_i} \tag{8}$$

Since the time sequence of sediment transport rate at the basin outlet is ordered by the successive calculation of sediment yield and sediment transport, the sediment transport rate in the previous period $\boldsymbol{S}(t-1)$ will not be affected by the sediment yield calculation $\boldsymbol{SS}(t)$ in the current period, and conversely, the changes of sediment yield

$$\begin{cases} \boldsymbol{S}(\boldsymbol{SS}, \theta, 1) \approx \boldsymbol{S}(\boldsymbol{SS}_C, \theta, 1) + \left.\frac{\partial \boldsymbol{S}(\boldsymbol{SS}_C, \theta, 1)}{\partial ss_1}\right|_{\boldsymbol{SS}=\boldsymbol{SS}_C}\Delta ss_1 + \left.\frac{\partial \boldsymbol{S}(\boldsymbol{SS}_C, \theta, 1)}{\partial ss_2}\right|_{\boldsymbol{SS}=\boldsymbol{SS}_C}\Delta ss_2 + \cdots + \left.\frac{\partial \boldsymbol{S}(\boldsymbol{SS}_C, \theta, 1)}{\partial ss_n}\right|_{\boldsymbol{SS}=\boldsymbol{SS}_C}\Delta ss_n \\ \boldsymbol{S}(\boldsymbol{SS}, \theta, 2) \approx \boldsymbol{S}(\boldsymbol{SS}_C, \theta, 2) + \left.\frac{\partial \boldsymbol{S}(\boldsymbol{SS}_C, \theta, 2)}{\partial ss_1}\right|_{\boldsymbol{SS}=\boldsymbol{SS}_C}\Delta ss_1 + \left.\frac{\partial \boldsymbol{S}(\boldsymbol{SS}_C, \theta, 2)}{\partial ss_2}\right|_{\boldsymbol{SS}=\boldsymbol{SS}_C}\Delta ss_2 + \cdots + \left.\frac{\partial \boldsymbol{S}(\boldsymbol{SS}_C, \theta, 2)}{\partial ss_n}\right|_{\boldsymbol{SS}=\boldsymbol{SS}_C}\Delta ss_n \\ \vdots \\ \boldsymbol{S}(\boldsymbol{SS}, \theta, L) \approx \boldsymbol{S}(\boldsymbol{SS}_C, \theta, L) + \left.\frac{\partial \boldsymbol{S}(\boldsymbol{SS}_C, \theta, L)}{\partial ss_1}\right|_{\boldsymbol{SS}=\boldsymbol{SS}_C}\Delta ss_1 + \left.\frac{\partial \boldsymbol{S}(\boldsymbol{SS}_C, \theta, L)}{\partial ss_2}\right|_{\boldsymbol{SS}=\boldsymbol{SS}_C}\Delta ss_2 + \cdots + \left.\frac{\partial \boldsymbol{S}(\boldsymbol{SS}_C, \theta, L)}{\partial ss_n}\right|_{\boldsymbol{SS}=\boldsymbol{SS}_C}\Delta ss_n \end{cases} \tag{5}$$

in the current period $\boldsymbol{SS}(t)$ will not influence $\boldsymbol{S}(t-1)$ through the dynamic system response in the SSC model. If $t < i$, then:

$$\frac{\partial \boldsymbol{S}(\boldsymbol{SS}, \theta, t)}{\partial ss_i} = 0 (t = 1, \cdots L; i = 1, \cdots, n) \tag{9}$$

Strengthening the correlation of the corrected values of slope sediment yield in each period and improving the stability of corrected consequences are of great importance. Thus, the error stationary matrix and stability constraints are incorporated into the unconstrained least squares method $\min_{\Delta SS} \boldsymbol{E}^T\boldsymbol{E}$. The stationary matrix of slope sediment yield error is written as:

$$\boldsymbol{A} = \begin{bmatrix} 1 & -1 & 0 & \cdots & 0 \\ 0 & 1 & -1 & \cdots & 0 \\ \vdots & \vdots & \vdots & \vdots & \vdots \\ 0 & 0 & \cdots & 1 & -1 \end{bmatrix} \begin{bmatrix} \frac{1}{ss_1} & & & \\ & \frac{1}{ss_2} & & \\ & & \ddots & \\ & & & \frac{1}{ss_n} \end{bmatrix},$$

then

$$(\boldsymbol{A}\Delta\boldsymbol{SS})^T(\boldsymbol{A}\Delta\boldsymbol{SS}) = \sum_{i=1}^{n-1} \left(\frac{\Delta ss_i}{ss_i} - \frac{\Delta ss_{i+1}}{ss_{i+1}} \right)^2 \tag{10}$$

where $\frac{\Delta ss_i}{ss_i}$ denotes the modified proportion of slope sediment yield. Accordingly, $\Delta\boldsymbol{SS}$ satisfies:

$$\min_{\Delta R} [\boldsymbol{E}^T\boldsymbol{E} + \beta(\boldsymbol{A}\Delta\boldsymbol{SS})^T(\boldsymbol{A}\Delta\boldsymbol{SS})] \tag{11}$$

where the weight coefficient β can be used to balance the two: the stability constraints and the sum of squared error. The value of β varies within different floods. The correction results are more stable with larger β, and its best performance is shown when β reaches a specific value. Moreover, no matter what value β is assigned, the corrected results will always maintain a certain correction effect. However, the optimal weight coefficients in real basins are often larger, mainly due to the complex conditions in real basins and the difficulty in extracting effective information (Liu *et al.* 2015).

Eventually, $\Delta\boldsymbol{SS}$ is obtained by Equation (6) and expressed as:

$$\Delta\boldsymbol{SS} = (\boldsymbol{U}^T\boldsymbol{U} + \beta\boldsymbol{A}^T\boldsymbol{A})^{-1}\boldsymbol{U}^T(\boldsymbol{S}(\boldsymbol{SS}, \theta, t) - \boldsymbol{S}(\boldsymbol{SS}_C, \theta, t)) \tag{12}$$

The additional term $\beta\boldsymbol{A}^T\boldsymbol{A}$ could control the range of change $\Delta\boldsymbol{SS}$, which helps to effectively alleviate or avoid the 'oscillation' phenomenon, and further enhance the stability of this correction method.

The corrected series of slope sediment yield $\boldsymbol{SS}'_C$ is computed as:

$$\boldsymbol{SS}'_C = \boldsymbol{SS}_C + \Delta\boldsymbol{SS} \tag{13}$$

Then the updated series of sediment transport rate processes $\boldsymbol{S}_U$ can be expressed as:

$$\boldsymbol{S}_U = \boldsymbol{S}_C + \boldsymbol{U}(\boldsymbol{SS}'_C - \boldsymbol{SS}_C) \tag{14}$$

where $\boldsymbol{S}_C$ is the calculated sediment transport rate before updating occurs.

Figure 4 provides a further explanation for performing the dynamic correction process. Observed rainfall $\boldsymbol{P}$, runoff $\boldsymbol{R}$, discharge $\boldsymbol{Q}(t)$ and sediment transport rate processes $\boldsymbol{S}(t)$ are shown as graphical information for the case contained in Figure 4. By using the DSRC method, corresponding corrected processes such as $\boldsymbol{S}_t(t)$, $\boldsymbol{S}_{t+i}(t)$ are generated by each original rainfall inputs series t, $t+i$ respectively. The ultimate updating process ($S_{t+1}(t)$ in Figure 4 is, therefore, dynamically corrected against an observed time series of input data.

The detailed steps for dynamic correction of sediment transport rate processes using the DSRC method are presented as follows: 1. Slope sediment yield $\boldsymbol{SS}_i (i = 1, \cdots, n)$ are first calculated by using the observed data of streamflow and sediment before the initial time t of rainfall (including current time), and therefore the calculated sediment transport rate series $\boldsymbol{S}_i(t)$ is acquired; 2. Calculated series $\boldsymbol{SS}_k (k \neq i)$ from the former computation are fixed to the constant values, while adding slope sediment yield $\boldsymbol{SS}_i$ by one step Δss_i. A new series of slope sediment yield $\boldsymbol{SS}'_i$ is then

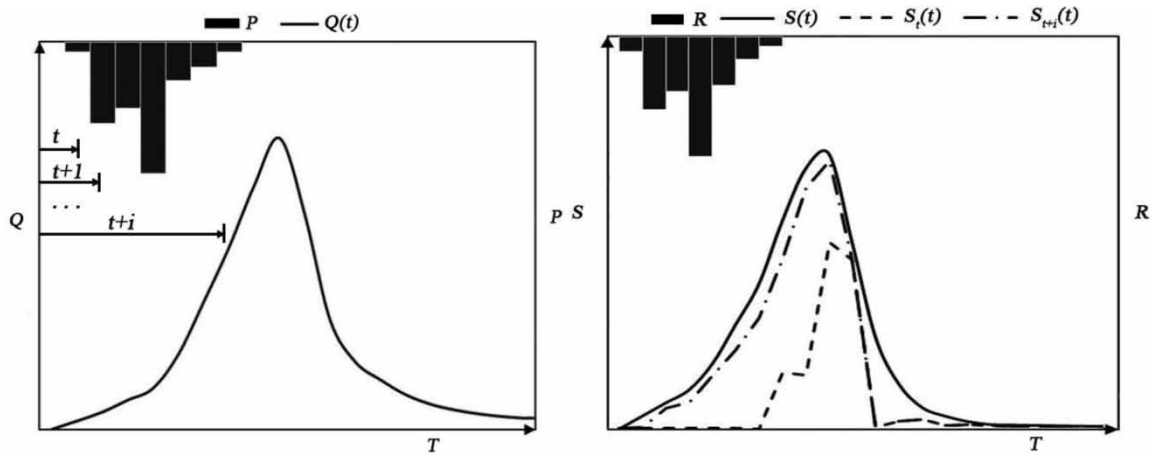

Figure 4 | Schematic diagram of dynamic correction processes for sediment transport rate.

obtained; 3. The new series $\boldsymbol{SS}_i'$ is applied to recalculate the sediment transport rate series $\boldsymbol{S}_i(t)'$; 4. The system response curves of $\boldsymbol{SS}_i$ are then computed from the differences between $\boldsymbol{S}_i(t)'$ and $\boldsymbol{S}_i(t)$ divided by the step Δss_i. Each column in the $\boldsymbol{U}$ matrix is obtained in the same way; 5. Based on the error correction method through DSRC mentioned above (Equations (5)–(14)), the new series of sediment transport rate is acquired. Moreover, only the value in the next moment $t+1$ of the original series $\boldsymbol{S}_i(t)$ calculated by the SSC model is substituted by the new computed one at the corresponding time. Therefore, the corrected (not the final) sediment transport rate process $\boldsymbol{S}_t(t)$ is obtained; 6. Steps 1–5 are repeated in the next correction period $t+1$ and terminated in the last period $t+i(i=1,\cdots,n)$ which is the end of rainfall in this flood. Eventually, the final corrected sediment transport rate process $\boldsymbol{S}_{t+i}(t)$ is obtained by continuous replacement over the range of correction spanned by the rainfall period.

Objective function criteria

In order to provide a statistical analysis of each correction in different flood events, it is necessary to identify multiple performance measures to evaluate the goodness-of-fit (Song *et al.* 2011). Three quantitative measures, including the Nash–Sutcliffe (*NS*) coefficient, the relative error of sediment peak and relative error of sediment yield are used to check the correction performance of the DSRC method. The level of effective improvement, in comparison to the results before correction, is measured by two quantitative indices with respect to sediment peak and NS improvement in both the ideal case and real-data simulation. Model performance is evaluated according to the following metrics:

1. Nash–Sutcliffe (*NS*) (Yapo *et al.* 1996):

$$NS = 1 - \sum_{i=1}^{N} [S_C(i) - S_O(i)]^2 / \sum_{i=1}^{N} [(S_O(i) - \overline{S_O}]^2 \tag{15}$$

2. The relative error of sediment peak (Bao *et al.* 2012):

$$\Delta SI_p = [(SI_{OP} - SI_{CP})/SI_{OP}] \times 100\% \tag{16}$$

3. The relative error of sediment yield:

$$\Delta SI = [(SI_O - SI_C)/SI_O] \times 100\% \tag{17}$$

4. The effective improvement of sediment peak:

$$\delta \hat{S}_P = 1 - \frac{|SI_{OP} - SI_{UP}|}{|SI_{OP} - SI_{CP}|} \tag{18}$$

5. The effective improvement of NS:

$$INS = 1 - \sum_{i=1}^{N} [S_O(i) - S_U(i)]^2 / \sum_{i=1}^{N} [(S_C(i) - S_O(i)]^2 \quad (19)$$

where S_C, S_O are computed and observed sediment transport rate (t/s); $\overline{S_O}$ is the mean value of observed sediment transport rate (t/s); N is the number of time periods in a flood event; SI_{CP}, SI_{OP}, SI_{UP} are calculated, observed and corrected sediment peak (t/s); SI_C, SI_O represent calculated and observed sediment yield respectively (t); T_{CP}, T_{op} represent computed and observed occurrence time of sediment peak (t/s); S_U denotes the corrected sediment transport rate calculated by the updated slope sediment yield (t/s); i is the number of time period. Terms $\delta\hat{S}_P$, INS are used to evaluate the relative effectiveness of the correction method. Note that larger values for $\delta\hat{S}_P$, INS mean that better improvements are achieved by updating and a maximum value is 1.0.

Model parameters

Twenty-two parameters of both streamflow and sediment parts in the SSC model are included. Floods in each basin used for calibration are event-based for which hourly streamflow and sediment datasets are available. To calibrate the model parameters, an optimization algorithm which merges the strengths of the auto-estimated method based on parameter function surface (Bao *et al.* 2013) is used. Three performance measures, the Nash–Sutcliffe efficiency (NS), relative error of sediment yield ΔSI and relative error of sediment peak ΔSI_P, are taken as the objective functions (Bardossy & Singh 2008; Wagener *et al.* 2009) to determine the optimal model parameters. The final calibrated parameter sets of streamflow and sediment are listed in Tables 3 and 4 and, once calibrated, generally do not change during both calculation and correction periods.

CASE STUDY AND RESULTS ANALYSIS

Ideal case

Input, output, parameters, initial states, and the sediment yield error are all known in the ideal case. A basin with a drainage area of 3,906 km^2 and 67 rainfall stations is used to estimate the corrected performance of the DSRC method. To ensure that the rainfall dataset $\boldsymbol{P}$ used is consistent with an actual storm situation, we selected data from a flood event in the Dali River basin on 11 August 1979. Since no actual observed sediment data is given in this case, the slope sediment yield $\boldsymbol{SS}_0$ calculated by the given rainfall dataset $\boldsymbol{P}$ is regarded as the 'observed' one. Thus, the 'observed' sediment transport rate $\boldsymbol{S}_0$ is calculated by the SSC model. The slope sediment yield error $\Delta\boldsymbol{SS}'$ (Figure 5) is set as a random series, and the assigned range of the slope sediment yield error is assumed to be constant in time. The magnitude of each error in the random error

Table 3 | Calibrated streamflow parameters of the SSC model in each study basin

Streamflow parameters	K	WM	WUM	WLM	C	FC	B	KI	KG	CS	CI	CG	KE	XE
Jiuyuangou	1	250.12	20	80	0.16	9.97	0.26	0.4	0.37	0.1	0.95	0.995	0.5	0.05
Chabagou	1	280.57	20	80	0.16	6.18	0.13	0.3	0.55	0.5	0.65	0.995	0.3	0.05
Dali River	1	251.36	20	80	0.1	7.45	0.16	0.4	0.37	0.6	0.65	0.995	0.5	0.05

Table 4 | Calibrated sediment parameters of the SSC model in each study basin

Sediment parameters	ACM	CM	REMM	BS	ζ	CSS	CGM	KXD	XS	KXG
Jiuyuangou	0.99	805.56	700	1	0.5	34.25	100	0.1	0.1	1.37
Chabagou	0.22	1,575.63	1,000	1	0.03	1.3	100	0.6	0.2	0.20
Dali River	0.82	1,200	1699029	1	0.01	3.30	123.24	0.1	0.3	0.64

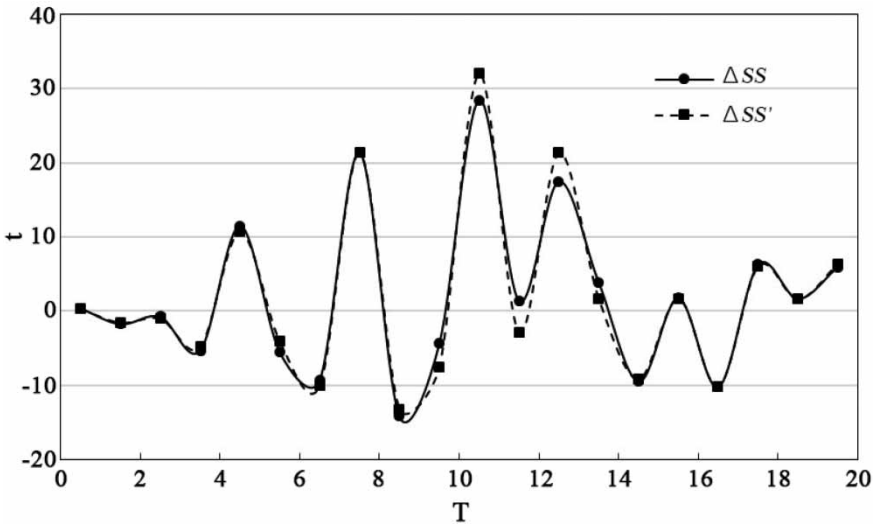

Figure 5 | Comparison of assigned and estimated error of slope sediment yield.

series is limited to a certain range of ±30% of the corresponding 'observed' slope sediment yield $\boldsymbol{SS}_0$. Since $\boldsymbol{SS}_0$ varies with time, the assigned sediment yield error therefore varies in time as well. By adding the assigned error to $\boldsymbol{SS}_0$ at the corresponding time period respectively, the calculated series of slope sediment yield $\boldsymbol{SS}_C$ is then acquired. $\boldsymbol{SS}_C$ is calculated by the following equation:

$$\boldsymbol{SS}_C = \boldsymbol{SS}_0 + \Delta\boldsymbol{SS}' \tag{20}$$

The calculated sediment transport rate $\boldsymbol{S}_C$ is obtained by the SSC model using the $\boldsymbol{SS}_C$ series. Assigned error $\Delta\boldsymbol{SS}'$ and estimated error $\Delta\boldsymbol{SS}$ (computed by the DSRC method) of slope sediment yield, along with their inter-correlation among the time period, is shown in Figures 5 and 6

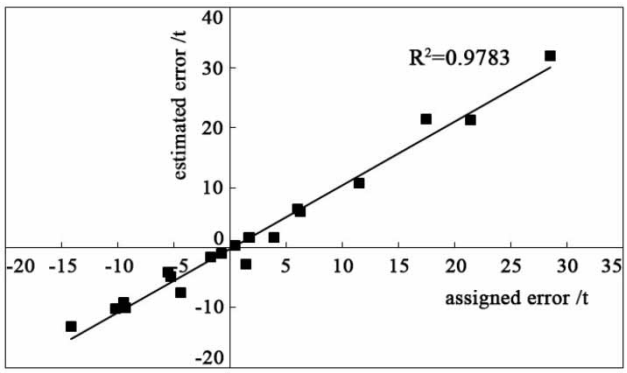

Figure 6 | Correlation between assigned and estimated error of slope sediment yield.

respectively. T is the number of time period. Though the two series are slightly different and varied with the corresponding slope sediment yield, the error values estimated by the DSRC method are very close to the actual (assigned) values. The correlation coefficient is 0.978 (Figure 6). Furthermore, the sum of slope sediment yield errors is 39.4 t, while that of the estimated series corrected by DSRC method reached 38.7 t – a relative error of only 1.9%.

In Figure 7, $\boldsymbol{R}$, $\boldsymbol{S}_C$, $\boldsymbol{S}_U$, $\boldsymbol{S}_O$ represent runoff depth, calculated, corrected, and observed sediment transport rate process respectively. As shown in Figure 7, the DSRC method significantly improves the forecast in sediment transport process compared to the original calculation. $\Delta\boldsymbol{SI}_P$ decreases from –11.60 to 2.56%, $\Delta\boldsymbol{SI}$ decreases from –3.33 to 0.04%, while NS coefficient increases from 0.978 to 0.998. Even when the sediment yield errors vary with time, the DSRC method could still accurately estimate the error series by extracting useful information from the observed data. The results reflect the fact that through accurate time-varying slope sediment yield error estimates, forecast accuracy in the sediment transport rate process at the basin outlet tends to be effectively improved using the DSRC method.

Real basin

The DSRC method is further tested in three real basins with different spatial scales and rain gauge densities.

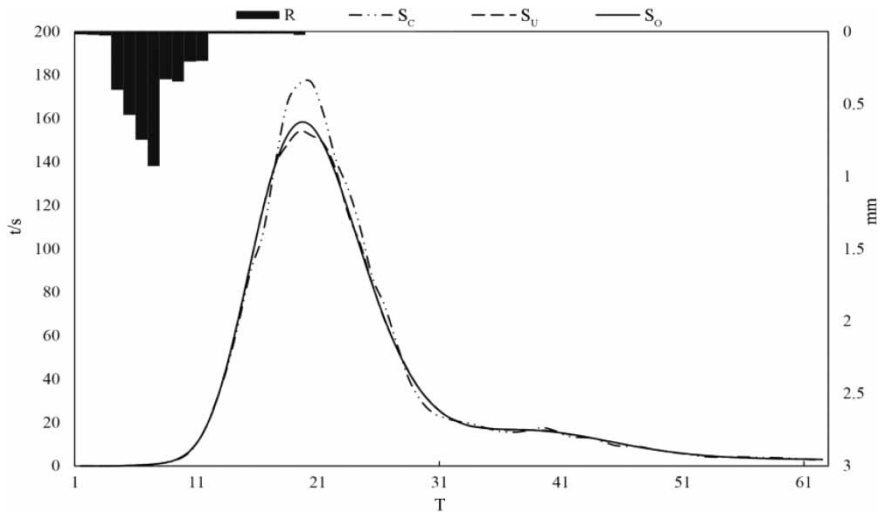

Figure 7 | Sediment transport rate process comparison of the ideal case.

The flood data and more detailed basin information used for each of the three cases are summarized in Table 5. In accordance with the national criteria for flood forecasting in China (MWR 2006), the results are acceptable (also known as qualified simulation) when the absolute errors between observed and corrected sediment yield in flood events are equal to or less than 30%. A value of ΔSI is acceptable when it shows a desirable limit within 30%, with '$\surd$' in the corresponding table; while '$\times$' indicates too much lower accuracy in simulation. The sediment yield and peak dominate the process characteristics and are thus more important for simulation, which is a better measure of how well the model corrects the overall sediment process. The observed, computed, and updated results of each basin are listed in the supporting information, Tables S1–S3.

Jiuyuangou basin

Over the 11 floods in supporting information Table S1, it can be noted that the DSRC method produces a higher *NS* value and a lower relative error of both sediment yield and peak than the initial calculation in nearly every correction. In this case, the average improvement in *NS* value has been increased from 0.500 to 0.849, with an average effective improvement in *NS* (*INS*) being 0.686. As shown in Figure 8(a), the *NS* performance metric values for the DSRC method are significantly larger than the *NS* of the SSC model without updating. That is, the DSRC updating method is effective at improving the forecast accuracy. The better *NS* performance is especially reflected in the decrease of relative error of sediment peak (from 49.69 to 8.70%) and in the decrease of relative error of sediment yield (from

Table 5 | Statistical information of historical floods in each study basin

Basin name	Area (km^2)	Number of rainfall stations	Average control area of rainfall station (km^2)	Data series (year)	Time step (min)	Annual average precipitation (mm)	Annual average sediment yield modulus t/(km^2·a)	Number of historic floods
Jiuyuangou	70.7	11	6.43	1959–1977	6	500	1.9×10^4	11
Chabagou	187	46	4.07	1960–2009	30	447	2.2×10^4	45
Dali River	3,906	67	58.30	1966–2013	30	440	1.6×10^4	45

23.36 to 13.48%). The improved qualified rate (the proportion of qualified floods) hence results from significantly better model forecasts (36.4% improvement).

Chabagou basin

Table S2 shows the comparison results concerning the sediment process focused precision indices. The accuracy has significantly improved when using the DSRC method over the period, whether human activities intervene or not. Specifically, the qualified rate has been increased from 84.4 to 97.8%, with an increment of 13.4%. Note that the average *NS* value of 45 historical floods improved from 0.442 to 0.929, and the value greater than 0.9 in flood events is 0 and 42 before and after correction, respectively. The *NS* values (before and after updating) for every flood event are shown in Figure 8(b). In all flood events, the *NS* performance is improved by updating, showing the significant updating effect of the DSRC method. For some floods like No. 19610926, sediment yield estimates seem to be overcorrected with the increasing relative error. On average, however, the relative error decreases from 23.74 to 11.56%. The mean relative error of sediment peak decreases from 56.87 to 9.99%, showing an effective improvement, as much as 0.719 on average.

Dali River basin

The corrected outcomes of Dali River basin also show consistency with that of other basins, however, relatively poor performance in sediment peak correction is obtained. Table S3 shows a direct comparison of the results. Note that the qualified rate is improved from 55.6 to 95.6% (40% improvement) and the average *NS* value is improved from 0.301 to 0.816 (0.515 improvement). *NS* values (before and after updating) for every flood event are compared in Figure 8(c). As shown in Figure 8(c), the accuracies of flood estimates for the 45 events in the Dali River basin have, again, been significantly improved by the DSRC updating method. The number of floods with *NS* greater than 0.9 increased from 0 to 7. Though the percentage of absolute error of corrected sediment peak falling within the qualified range of <30% decreased from 33.46 to 19.99%, the negative percentage indicates the corrected mean value exceeds the observed one. The mean effective improvement in *NS* value reaches 0.696, whereas the improvement of sediment peak is less effective due to overcorrection. Overcorrection also remains in some floods, while the mean relative error of sediment yield still decreases from 34.73 to 19.01%.

Results analysis

According to the results obtained in different basins (listed in the supporting information), the DSRC method has been proven as a useful tool for improving the accuracy of real-time flood predictions. This method has a significant correction effect for both sediment peak and total sediment yield. This is the case for both smaller and larger basin scales. Besides, the improvements in the three study basins vary with basin size and rain gauge density. A larger relative (percentage) improvement is obtained for larger basin scales, and the mean *NS* value gradually increases with increasing rain gauge density. Though the DSRC method is effective and stable at improving the forecast accuracy for the sediment transport process, the corrected relative error of sediment yield of some floods is slightly larger than that without updating.

Chabagou basin is chosen as the target basin for further statistical analysis. Unqualified flood No. 19950904 is considered for its poor performance in the relative error of sediment yield over 30% without proper correction to sediment peak (listed in the supporting information Table S2). The initial error of calculated sediment peak can be partially linked to the stationary assumption of parameters like ξ, *KXD* and *KXG* in the sediment transport phase. Moreover, the uncorrected peak value indicates that the short rainfall duration leads to a short correction period before peak time. The short correction period has restricted the use of effective observed information for tracking errors by the DSRC method, and therefore incurs a much lower *NS* value (only 0.313), but still 0.097 higher than that before correction.

Four typical floods in Chabagou basin (No. 19680813, No. 19730630, No. 19890721, and No. 20060730, including human intervention periods) are presented in Figure 9 to reveal the corrective effectiveness of the DSRC method. Except for No. 20060730, the relative error of sediment

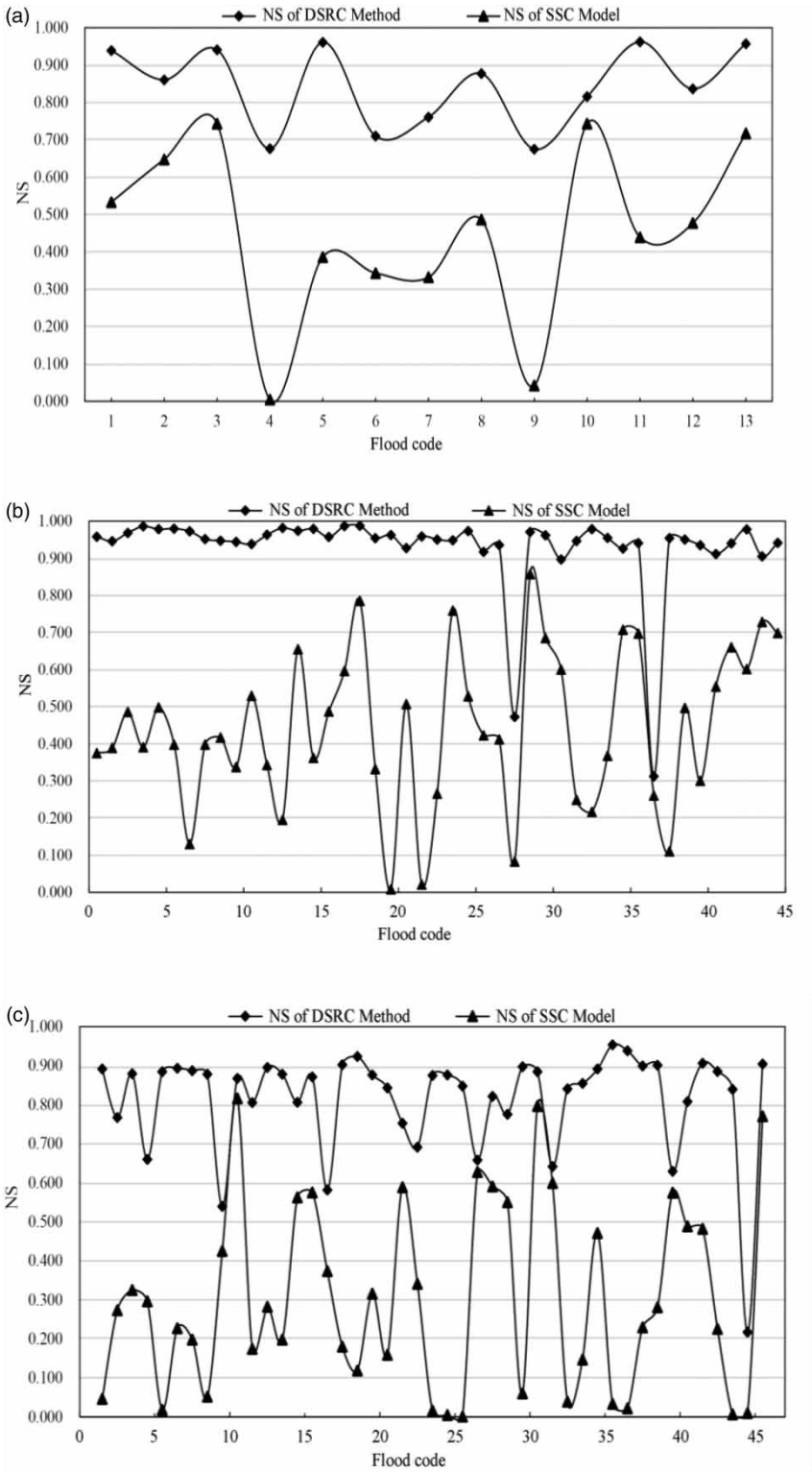

Figure 8 | NS performance values (before and after updating) for basins. (a) Jiuyuangou basin, (b) Chabagou basin, (c) Dali River basin.

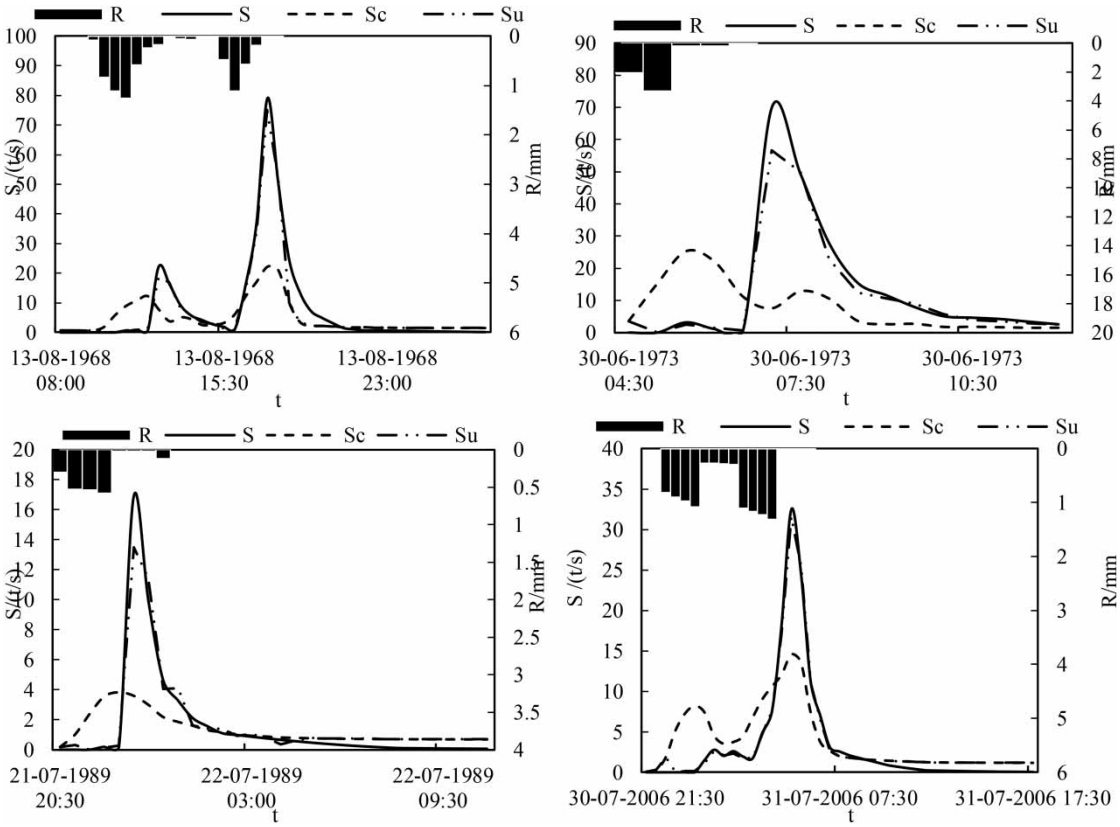

Figure 9 | Comparison between observed and calculated sediment rate process of four typical floods (where R is runoff depth, S is observed sediment transport rate process, S_C is the primary process computed by model, and S_U is the corrected process by DSRC).

yield is reduced among the above four floods. As shown in Figure 9, the estimates of the sediment transport rate process at the basin outlet have been effectively corrected through a process of estimating the time-varying size of the slope sediment yield error. For the selected four floods, peak values are obviously corrected without time difference. The *NS* value is increased from 0.487 to 0.957, from 0.008 to 0.962, from 0.249 to 0.929 and from 0.601 to 0.978, respectively, while the significant improvement in sediment peak brings about the increased relative error of sediment yield in No. 20060730. It is worth noting here that a better simulation of rising and falling stages is achieved, which supports the view that the DSRC method can obtain sufficient effective information for identifying errors.

With respect to the comparison of the correction effect of each basin, performance statistics for non-updated and updated sediment processes are shown in Table 6 (ranked in order of ascending size of drainage area). Overall, in all real cases, better effectiveness by using the DSRC method for updating in both quantity and processes is achieved.

Table 6 | Statistical tables of corrective effects for each study basin

		SSC model					DSRC method						
Basin	**Flood events**	$\overline{NS}$	ΔSI (%)	ΔSI_P (%)	**Qualified rate (%)**	**NS** ≥ 0.9	$\overline{NS}$	ΔSI (%)	ΔSI_P (%)	**Qualified rate (%)**	**NS** ≥ 0.9	**INS** ≥ 0.5	$\delta\widehat{SP} \geq 0.5$
Jiuyuangou	11	0.500	23.36	49.69	63.6	0	0.849	13.48	8.70	100	4	9	11
Chabagou	45	0.442	23.74	56.87	84.4	0	0.929	11.56	9.99	97.8	42	43	39
Dali River	45	0.301	34.73	33.46	55.6	0	0.816	19.01	–19.99	95.6	7	36	23

Qualified rates of the DSRC method are all more than 90% with the highest improvement in Dali River basin (represents 41.8%). The average *NS* values after updating are all greater than 0.8 meaning a good-of-fitness in process forecasting, while the least increment of 0.349 is in Jiuyuangou basin and the greatest increment of 0.515 is in Dali River basin. Meanwhile, sediment yield estimates of some floods within the study basins seem to be overcorrected. This is primarily explained by the fact that the sediment peak is significantly improved. Such results also provide an indication of the limited use of effective information for forecast correction. However, the overall trend is the decreasing error in simulation, indicating that improved accuracy is acquired in real-time flood forecasting when using the DSRC method. As shown in Table 6, the decrement of the relative error of sediment yield increases with increasing basin area; 9.88% in Jiuyuangou basin, 12.18% in Chabagou basin, and 15.72% in Dali River basin. Furthermore, it is worth mentioning that the correction effect of sediment yield tends to be less stable compared to the improvement on the peak, the choice of objective function could be a decisive factor.

For the DSRC method, the updating effect is more significant for larger basins and for basins with lower rain gauge densities. According to the indices *INS* and $\delta\hat{S}_P$, in contrast to the performance of Chabagou basin, Jiuyuangou and Dali River basins perform less well in terms of *NS* performance and sediment peak correction. An important reason being that the reducing rainfall station density brings about decreasing quality of mean areal precipitation input data. For basins with lower rain gauge densities, the location of the storm center and the distribution of rainfall intensities are more difficult to monitor, resulting in a tendency to misrepresent the amount of actual rainfall falling over the basin. The information for each basin is listed in Table 5; note that the largest effective rainfall gauge area (smallest density of rainfall stations) is in the Dali River basin (58.30 km^2/Gauge) while the least (largest density) is in Chabagou basin (4.07 km^2/Gauge). Thus, less satisfying corrected results for sediment simulation of Dali River basin are received. However, the Dali River basin results in much larger improvements to the corrected performance, due to the lower accuracies of the original flood estimates. This view could also be further supported by more study results in Si *et al.* (2015). Correction in much smaller basin areas (Jiuyuangou basin in this study) where sediment concentration time is short seems to get less satisfying performance than larger ones due to its lack of using effective information. In summary, the error feedback correction based on DSRC provides ways to track errors by using observed and calculated information. For real cases with different basin scales, improved sediment yield estimates result in improved forecast accuracy that then correct forwards in time to reduce future sediment transportation errors. Moreover, the sensitivity of results to rainfall station density would become a good channel to further investigate the correction effect for sediment yield of the DSRC method.

CONCLUSIONS AND DISCUSSION

The streamflow-sediment coupled model is simple, the model parameters are easily calibrated, and the model structure is physics-based. Compared with mathematical models (De Roo & Jetten 1999; Ramsankaran *et al.* 2013; Juez *et al.* 2018a, 2018b), the SSC model is not restricted to study watersheds where there has been considerable work undertaken for the description of the watershed and necessary inputs. The physical model structure can be simplified to reflect the key processes by considering the time-varying factors in structure and reflecting the time-invariant factors by parameters (Bao 1995; Bao & Wang 1997). It has been successfully used to predict streamflow and sediment transport processes in the loess region, whereas the results in the sediment simulation are more or less unsatisfactory. A real-time error correction method is needed to decrease the error of forecasting. The DSRC method, therefore, been developed and incorporated into the SSC model to correct the slope sediment yield error for improving sediment transport forecasts. The theoretical basis for the approach is the local (i.e. at current conditions) sensitivity of the system response to perturbations in the sediment yield time series. The DSRC method has the following advantages: it is simple and the performance indices will not deteriorate as the forecasting period increases. Furthermore, it is based on physical mechanisms and will not increase either the number of model parameters or model complexity.

Ideal and three real-data cases, over the range spanned by different scales of basin areas, are used to verify the effectiveness of the proposed DSRC method. Results of all cases show the accuracies of flood forecasts are greatly improved by the DSRC method. The analysis of improvement further confirms that the SSC model performs with a sound physical structure of sediment transport. This method has a significant correction effect for both sediment peak and total sediment yield. The limitation of effective information for error estimates use is the direct factor which leads to the poor performance. Meanwhile, the improvements vary with basin size and rain gauge density (as reported also by Si *et al.* (2015)), which is mainly attributed to the larger uncertainties in estimates of sediment yield error resulting from larger basins and lower rainfall station densities. Moreover, the gain decreases with the increase in rainfall station densities. Over the human intervention period when there are many water conservancy projects and measures involved within the basins, the DSRC method also presented a significant corrective effect to the flood forecasts.

Overall, the DSRC method merges the strengths of error tracing and feedback with the utilization of effective information. It can be directly applied to both linear and nonlinear hydrological model structures. DSRC is a comprehensive correction method, which means that it can be used to input, state, and output correction in real-time updating. The improvement of sediment prediction accuracy has direct relevance for guiding streamflow-sediment forecasting, river management and for reservoirs operation in the loess plateau area of the Yellow River. Therefore, the newly developed method is a reasonable and effective sediment yield correction method for real-time flood forecasting. While the DSRC method provides a definite improvement in performance, some forecasts are slightly overcorrected. The correction effect varies greatly with the objective function used, and the sediment balance information in the choice of objective function would require further consideration. Further ways can be explored to optimize model parameters calibration based on the DSRC method. More extensive work will continue to further evaluate the effectiveness of the DSRC method for real-time streamflow-sediment forecast updating widely, and to specifically quantify the uncertainty of sediment yield in the future.

ACKNOWLEDGEMENTS

This work was supported by the Fundamental Research Funds for Central Universities (B200201027), the National Natural Science Foundation of China (No.51709077), the Open Research Fund of Yellow River Sediment Key Laboratory (201804), Special Foundation for National Program on Key Basic Research Project (2016YFC0402703), and the Management of Central Public-Interest Scientific Institution Basal Research Fund (HKY-JBYW-2017-12).

DATA AVAILABILITY STATEMENT

All relevant data are included in the paper or its Supplementary Information.

REFERENCES

Babovic, V., Rene, H. J. & Klinting, A. 2001 Neural networks as routine for error updating of numerical models. *J. Hydraul. Eng.* **127** (3), 181–193.

Bagnold, R. A. 1960 Sediment discharge and stream power – a preliminary announcement. *US Geol. Circ.* **421**, 23–51.

Bao, W. M. 1995 A conceptual streamflow-sediment coupled simulation model for small basins. *Geogr. Res.* **14** (2), 27–34.

Bao, W. M. 2006 *Hydrological Forecasting*. China Water Power, Beijing, pp. 222–245.

Bao, W. M. & Wang, C. L. 1997 Vertically-mixed runoff model and its application. *Hydrology* **3**, 18–21.

Bao, W. M., Si, W., Shen, G. H., Zhang, X. Q. & Li, Q. 2012 Runoff error updating based on unit hydrograph inversion. *Adv. Water Sci.* **23** (3), 317–322.

Bao, W. M., Zhang, X. Q. & Zhao, L. P. 2013 Parameter estimation method based on parameter function surface. *Sci. Chin. Technol. Sci.* **56** (6), 1485–1498.

Bao, W. M., Si, W. & Qu, S. 2014 Streamflow updating in real-time flood forecasting based on runoff correction by a dynamic system response curve. *J. Hydrol. Eng.* **19** (4), 747–756.

Bao, W. M., Que, J. J., Lai, S. Z. & Si, W. 2015 Free-water storage error correction based on dynamic system response in flood forecasting. *Adv. Water Sci.* **26** (3), 365–371.

Bao, W. M., Hou, L., Shen, D. D. & Ni, Y. X. 2019 Application of streamflow-sediment coupled model in Dali River Basin of Loess Plateau. *J. Lake Sci.* **31** (4), 1120–1131.

Bardossy, A. & Singh, K. 2008 Robust estimation of hydrological model parameters. *Hydrol. Earth Syst. Sci.* **5** (3), 1641–1675.

Bingner, R. L., Garbrecht, J., Arnold, J. C. & Srinivasan, R. 1997 Effect of watershed subdivision on simulation runoff and fine sediment yield. *Trans. ASAE* **40** (5), 1329–1335.

Chen, L., Zhang, Y., Zhou, J., Vijay, P., Singh Guo, S. L. & Zhang, J. H. 2015 Real-time error correction method combined with combination flood forecasting technique for improving the accuracy of flood forecasting. *J. Hydrol.* **521**, 157–169.

De Chant, C. M. & Moradkhani, H. 2012 Examining the effectiveness and robustness of sequential data assimilation methods for quantification of uncertainty in hydrologic forecasting. *Water Resour. Res.* **48** (4), W04518.

De Roo, A. & Jetten, V. 1999 Calibrating and validating the LISEM model for two data sets from the Netherlands and South Africa. *Catena* **37** (3), 477–493.

De Vente, J. & Poesen, J. 2005 Predicting soil erosion and sediment yield at the basin scale: scale issues and semi-quantitative models. *Earth Sci. Rev.* **71** (1), 95–125.

De Vente, J., Poesen, J., Bazzoffi, P., Rompaey, A. & Verstraeten, G. 2010 Predicting catchment sediment yield in Mediterranean environments: the importance of sediment sources and connectivity in Italian drainage basins. *Earth Surf. Process. Landf.* **31** (8), 1017–1034.

Fang, H. Y., Cai, Q. G., Chen, H. & Li, Q. Y. 2008 Effect of rainfall regime and slope on runoff in a gullied loess region on the Loess Plateau in China. *Environ. Manage.* **42**, 402–411.

Gupta, H. V., Wagener, T. & Liu, Y. 2008 Reconciling theory with observations: elements of a diagnostic approach to model evaluation. *Hydrol. Process.* **22** (18), 3802–3813.

Gupta, H. V., Clark, M. P., Vrugt, J. A., Abramowitz, G. & Ye, M. 2012 Towards a comprehensive assessment of model structural adequacy. *Water Resour. Res.* **48**, W08301. doi:10.1029/2011WR011044.

Hairsine, P. B., Sander, G. C., Rose, C. W. & Parlange, J. Y. 1999 Unsteady soil erosion due to rainfall impact: a model of sediment sorting on the hillslope. *J. Hydrol.* **220** (3–4), 115–128.

Jiao, J. Y., Li, J. & Wang, W. Z. 2002 Erosion environment in the sediment-rich area on the Loess Plateau. *J. Geogr. Sci.* **12** (1), 49–57.

Ju, Q., Yu, Z. B., Hao, Z. C., Ou, G. X., Zhao, J. & Liu, D. D. 2009 Division-based rainfall-runoff simulations with BP neural networks and Xinanjiang model. *Neurocomputing* **72** (13), 2873–2883.

Juez, C., Hassan, M. A. & Franca, M. J. 2018a The origin of fine sediment determines the observations of suspended sediment fluxes under unsteady flow conditions. *Water Resour. Res.* **54**, 5654–5669.

Juez, C., Tena, A., Fernández-Pato, J., Batalla, R. J. & García-Navarro, P. 2018b Application of a distributed 2D overland flow model for rainfall/runoff and erosion simulation in a Mediterranean watershed. *Cuad. Investig. Geogr.* **44** (2), 615–640.

Komma, J., Bloschl, G. & Reszler, C. 2008 Soil moisture updating by ensemble Kalman filtering in real-time flood forecasting. *J. Hydrol.* **357** (3), 228–242.

Liu, K. X., Bao, W. M., Zhao, X. Q., Li, J. J., Que, J. J. & Shu, H. L. 2015 A system response correction method with runoff error smooth matrix. *J. Hydraul. Eng.* **46** (8), 960–966.

Merritt, W. S., Letcher, R. A. & Jakeman, A. J. 2003 A review of erosion and sediment transport models. *Environ. Model. Softw.* **18** (8–9), 761–799.

Ministry of Water Resources (MWR) 2006 *Regulation for Calculating Design Flood of Water Resources and Hydropower Projects*. Chinese Shuili Shuidian Press, Beijing (in Chinese).

Moradkhani, H., De Chant, C. M. & Sorooshian, S. 2012 Evolution of ensemble data assimilation for uncertainty quantification using the particle filter-Markov chain Monte Carlo method. *Water Resour. Res.* **48**, W12520. doi:10.1029/2012WR012144.

Neal, J. C., Atkinson, P. M. & Hutton, C. W. 2009 Evaluating the utility of the ensemble transform Kalman filter for adaptive sampling when updating a hydrodynamic model. *J. Hydrol.* **375** (3–4), 589–600.

Nearing, M. A., Jetten, V., Baffaut, C., Cerdan, O., Couturier, A. & Hernandez, M. 2005 Modeling response of soil erosion and runoff to changes in precipitation and cover. *Catena* **61** (2–3), 131–154.

Palazon, L., Gaspar, L., Latorre, B., Blake, W. H. & Navas, A. 2014 Evaluating the importance of surface soil contributions to reservoir sediment in alpine environments: a combined modelling and fingerprinting approach in the Posets-Maladeta Natural Park. *Solid Earth* **5** (2), 963–978.

Pegram, G. G. S. & James, W. 1972 Multilag multivariate autoregressive model for the generation of operational hydrology. *Water Resour. Res.* **8** (4), 1074–1076.

Qi, J. Y., Cai, Q. G., Cai, L. & Sun, L. Y. 2011 Scale effect of runoff and sediment reduction effects of soil and water conservation measures in Chabagou, Dalihe and Wudinghe Basins. *Prog. Geogr.* **30** (1), 95–102.

Ramsankaran, R., Kothyari, U. C., Ghosh, S. K., Malcherek, A. & Murugesan, K. 2013 Physically-based distributed soil erosion and sediment yield model (DREAM) for simulating individual storm events. *Hydrol. Sci. J.* **58** (4), 872–891.

Rompaey, A. V., Govers, G. & Puttemans, C. 2010 Modelling land use changes and their impact on soil erosion and sediment supply to rivers. *Earth Surf. Process. Landf.* **27** (5), 481–494.

Rouhipour, H., Ghadiri, H. & Rose, C. W. 2006 Investigation of the interaction between streamflow-driven and rainfall-driven erosion processes. *Aust. J. Soil Res.* **44** (5), 503–514.

Si, W., Bao, W. M., Wang, H. Y. & Qu, S. M. 2013a The research of rainfall error correction based on system response curve. *Appl. Mech. Mater* **368–370**, 335–339.

Si, W., Bao, W. M. & Qu, S. M. 2013b Runoff error correction in real-time flood forecasting based on dynamic system response curve. *Adv. Water Sci.* **24** (4), 497–503.

Si, W., Bao, W. M. & Gupta, H. V. 2015 Updating real-time flood forecasts via the dynamic system response curve method. *Water Resour. Res.* **51** (7), 5128–5144.

Si, W., Yu, H. H., Bao, W. M., Qu, S. M. & Zhang, Q. 2016 Area-mean rainfall updating by system response curve method and

application to real-time flood forecasting of Fuchunjiang basin. *J. Hydroelectric Eng.* **35** (1), 38–45.

Si, W., Bao, W. M., Jiang, P., Zhao, L. P. & Qu, S. M. 2017 A semi-physical sediment yield model for estimation of suspended sediment in loess region. *Int. J. Sediment Res.* **32** (1), 12–19.

Si, W., Gupta, H. V., Bao, W. M., Jiang, P. & Wang, W. Z. 2019 Improved dynamic system response curve method for real-time flood forecast updating. *Water Resour. Res.* **55** (9), 7493–7519.

Song, X. M., Kong, F. Z. & Zhu, Z. X. 2011 Application of Muskingum routing method with variable parameters in ungauged basin. *Water Sci. Eng.* **4** (1), 1–12.

Tamene, L., Park, S. J., Dikau, R. & Vlek, L. G. 2010 Reservoir siltation in the semi-arid highlands of northern Ethiopia: Sediment yield-catchment area relationship and a semi-quantitative approach for predicting sediment yield. *Earth Surf. Process. Landf.* **31** (11), 1364–1383.

Vrugt, J. A., Gupta, H. V., Nuallain, B. & Bouten, W. 2006 Real-time data assimilation for operational ensemble streamflow forecasting. *J. Hydrometeorol.* **7** (3), 548–565.

Wagener, T., Werkhoven, K. V. & Reed, P. 2009 Multi-objective sensitivity analysis to understand the information concert in stream streamflow observations for distributed watershed modeling. *Water Resour. Res.* **45** (2), 1–5.

Wang, D., Li, Z. B., Li, P., Gao, H. D., Zhao, B. H. & Yuan, S. L. 2016a Evaluation of overall distribution of check dam system in the Jiuyuangou Watershed. *Res. Soil Water Conserv.* **23** (5), 49–55.

Wang, H., Li, Z. B., Ma, B., Xiao, J. B. & Zhang, L. T. 2016b Characteristics of waters transformation in the hilly and gully regions of the Loess Plateau: A case study of the Jiuyuangou watershed. *Sci. Soil Water Conserv.* **14** (3), 19–25.

Weerts, A. H., Serafy, E. L. & Ghada, Y. H. 2006 Particle filtering and ensemble Kalman filtering for state updating with hydrological conceptual rainfall-runoff models. *Water Resour. Res.* **42** (9), 123–154.

World Meteorological Organisation (WMO) 1992 *Simulated Real-Time Intercomparison of Hydrological Models*. Operational Hydrology Rep. No. 38. WMO, Geneva.

Wu, L., Jiang, J., Li, G. X. & Ma, X. Y. 2018 Characteristics of pulsed runoff-erosion events under typical rainstorms in a small watershed on the Loess Plateau of China. *Sci. Rep.* **8** (1), 1–12.

Xian, M. Z., Yu, S. L., Xiang, L. P. & Shu, G. Z. 1983 Soils of the loess region in China. *Geoderma* **29** (3), 237–255.

Yang, S. S., Bao, W. M., Yang, X. Q., Que, J. J., Shu, H. L. & Li, J. J. 2015 The application of differential response in rainfall error correction. *Chin. Rural Water Hydropower* **2015** (1), 75–79.

Yapo, P. O., Gupta, H. V. & Sorooshian, S. 1996 Automatic calibration of conceptual rainfall-runoff models: sensitivity to calibration data. *J. Hydrol.* **181** (1–4), 23–48.

Zhang, O. Y., Feng, X. & Xu, J. X. 2007 Impacts of flood events in coarse sediment producing areas on channel siltation and fluvial process of the lower Yellow River. *Int. J. Sediment Res.* **22** (2), 142–149.

Zhang, L., Shi, C. X. & Zhang, H. 2010 Effects of check-dams on sediment storage-release in Chabagou watershed. *Trans. Chin. Soc. Agric. Eng.* **2010** (2), 64–69.

Zhang, X. Q., Liu, K. X., Bao, W. M., Li, J. J. & Lai, S. Z. 2014 Runoff error proportionality coefficient correction method based on system response. *Adv. Water Sci.* **2014** (6), 24–31.

Zhao, R. J. 1993 A non-linear system for basin concentration. *J. Hydrol.* **142** (7), 477–482.

First received 2 December 2019; accepted in revised form 11 September 2020. Available online 27 October 2020